Adaptive and automatic diffraction orders filtering by singular value decomposition in off-axis digital holographic microscopy

PASQUALE MEMMOLO,[1,*] VITO RENÒ,[2] ETTORE STELLA[2], AND PIETRO FERRARO[1]

[1]*Istituto di Scienze Applicate e Sistemi Intelligenti "E. Caianiello" (ISASI-CNR), via Campi Flegrei 34, 80078 Pozzuoli (NA), Italy.*
[2] *Istituto di Sistemi e Tecnologie Industriali Intelligenti per il Manifatturiero Avanzato (STIIMA-CNR), via Amendola 122 D/O, 70126 Bari (BA), Italy.*
*p.memmolo@isasi.cnr.it

Abstract: Digital holography is a widely used in many fields for imaging, display and for metrology by exploiting its the capability furnish quantitative phase contrast map. The entire processing pipeline that permits to achieve phase-contrast images can be obtained by a cascade of numerical processing, such as the zero-order and twin image suppression, the automatic refocusing, the phase extraction by aberrations compensation and, if necessary, the phase unwrapping. In this paper, we propose a new method, based on the Singular Value Decomposition (SVD) filtering, to suppress zero-order and twin image in off-axis configuration, thus selecting automatically the desired real diffraction order. Actually, we demonstrate the proposed approach in the case of lack of knowledge about the reference beam's frequency and curvature, which typically occurs in portable off-axis holographic microscope systems for lab-on-a-chip applications. We validate the proposed strategy by a comparison with the common Fourier spatial filtering in the case of different experimental conditions and for several biological samples.

1. Introduction

Digital Holography (DH) in microscopy is a widely used imaging modality to access to label-free, full-field and Quantitative Phase Imaging (QPI) of biological samples as well as three dimensional (3D) sensing, 3D imaging, 3D Visualization, 3D display and others metrology applications [1-4]. In the last decade, several applications have been possible thanks to QPI by DH, such as lab on a chip analytical tools [5-7], high-throughput holographic 3D particles tracking [8,9], optical tomography [10-13], sick cells and diseases identification [14-16], just to name a few. In all of these applications, it is required to process recorded digital holograms to extract the quantitative phase information. The entire processing pipeline that permits to achieve phase-contrast images can be obtained by a cascade of numerical processing, such as the zero-order and twin image suppression, the automatic refocusing, the phase extraction by aberrations compensation and, if necessary, the phase unwrapping. All of these steps are widely investigated and very impressive amount of scientific contributions has been published in the last decade. In particular, zero-order and twin image suppression approaches in off-axis DH are typically based on suitable spatial filtering to be applied on the image of the Fourier transform of digital holograms [17-20]. This process aims to remove the carrier frequency of the reference beam used in the off-axis DH recording, thus demodulating and extracting the desired diffraction order term. The automatic focusing in DH consists in searching global extrema of suitable amplitude or phase sharpness metrics [21-23]. After the refocusing step, the phase reconstruction can be calculated from the complex amplitude and a

processing step concerning the aberration compensation is employed [24-26]. Finally, the phase reconstruction can need to be unwrapped if the recorded object provides over 2π phase variation [27,28]. Recently, all of these processing steps have been addressed by using the deep learning-based methods [29-32]. which provide accurate results but they are limited to the trained model, i.e. they work efficiently only for digital holograms recorded in the same or at most similar configuration of ones using for training the neural network. Since all of the aforementioned processing steps work in cascade, the overall quality and accuracy of one process is strictly related to those of previous one, thus making the zero-order and twin image suppression the fundamental step to assure high quality holographic reconstructions.

Here, we propose a general and robust approach to the zero-order and the twin image filtering out, thus providing accurate results for several off-axis holographic microscopy recording configurations and without any *a priori* knowledge about the reference beam aberrations, i.e. the carrier frequency used to implement the off-axis recording neither the beam curvature.

The proposed method provides an exact calculation of the carrier frequency of the reference beam by identifying the back focal plane (BFP) of the Microscope Objective (MO) exploiting the sparsity property of digital holograms [23]. Then, a Singular Value Decomposition (SVD) based filtering is applied on the Fourier transform of a digital hologram and the desired diffraction order is completely demodulated by subtracting the carrier frequency and by masking the Fourier spectrum with the SVD filter. It is important to note that, we consider the general case of different curvatures between object and reference beams, which typically occurs in field-portable holographic microscope devices for application at the lab-on-a-chip scale in which only one MO on the object beam is used. We validate the proposed approach in different experimental cases and compare it with the classical no-reference Fourier filtering strategy.

2. Proposed method

We consider digital holograms recorded in an off-axis digital holography microscope in which no information about the reference beam employed during the recording are available. In other words, the carrier frequency employed to implement the off-axis configuration, along with the beam aberrations, are unknown. The proposed approach for the automated extraction of the desired diffraction order consists of two main steps. The first one concerns the calculation of such carrier frequency, while the second step is devoted to the design of the optimal mask to extract the desired diffraction order. In the following two sub-sections, the detailed description about such two steps is reported.

2.1 Recovering the reference beam's carrier frequency

The carrier frequency in the digital holography in off-axis configuration is established by an appreciable angle between the object and reference beams. It can be easy to recover the real diffraction order if beams interfere having the same wavefront's curvatures. In fact, the amplitude Fourier spectrum provides three spatial frequencies with higher intensities, corresponding to the carrier frequencies of the three diffraction orders. Therefore, by selecting the desired one, it is possible to demodulate the digital hologram by shifting the real order's spectrum in the image center of the related Fourier spectrum. Then, by applying a circular mask, with a radius equal to the spectrum band, it is possible to select the real order.
In our investigation, the difference in wavefront's curvatures causes a defocusing of both real and twin spectrums, thus making unfeasible the demodulation process. An example of these two situations is reported in Fig.1, i.e. when wavefront's curvatures match (Fig.1a) or not (Fig.1b).

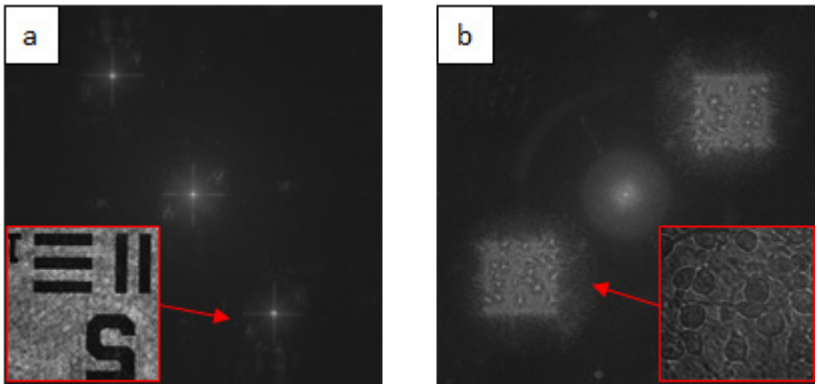

Fig. 1. Amplitude Fourier spectrums show the three diffraction orders appearance in the case of object and reference wavefront's curvature matched (a) and not (b). The inset figures report the corresponding digital holograms and the red arrows indicate the desired real diffraction orders.

The recovery of the carrier frequency for the example reported in Fig.1b, as well as for all digital holograms having defocused real and twin Fourier spectrums, can be obtained by an automatic process consisting of the search of the Back Focal Plane (BFP) of the microscope objective used in the recording setup. In fact, the BFP corresponds to the hologram's reconstruction plane proportional to the Fourier spectrum. Therefore, the BFP's reconstruction distance, to be used in the numerical diffraction Fresnel propagation integral, needs to be calculated. In ref. [23] it has been demonstrated that the BFP can be calculated by maximizing a suitable image contrast metric, such as the Tamura Coefficient (TC), defined as

$$TC_d = \sqrt{\frac{\sigma(\mathbf{A}_d)}{\mu(\mathbf{A}_d)}} \tag{1}$$

where $\mathbf{A}_d$ is the amplitude reconstruction calculated at distance d, $\sigma(.)$ and $\mu(.)$ are the standard deviation and average operators, respectively.

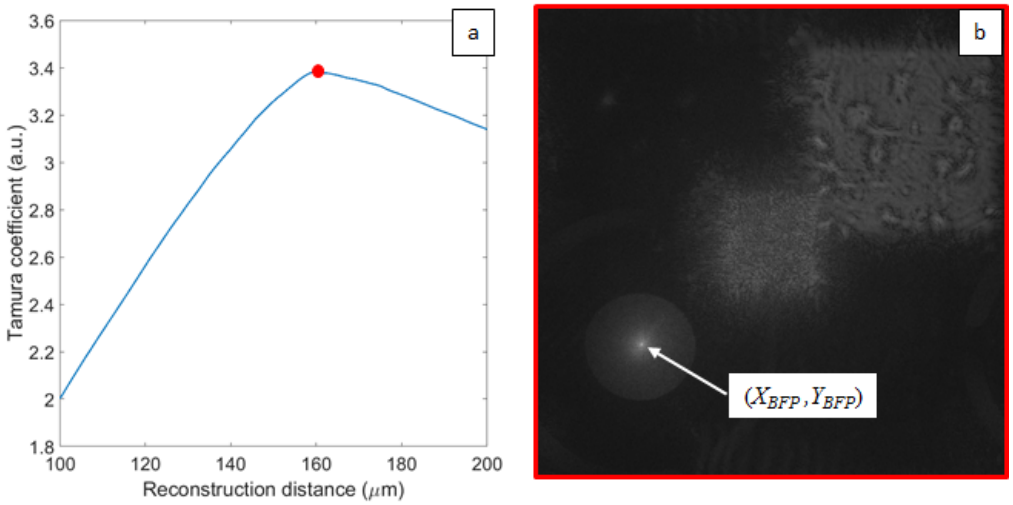

Fig. 2. BFP recovery by TC maximization. (a) the TC trend shows the global maximum at distance d=163μm, corresponding to the BFP reconstruction in (b). The coordinates (X_{BFP} ,Y_{BFP}) highlight the calculated carrier frequency.

By applying this approach to the digital hologram in Fig.1b we obtain the BFP reconstruction. In Fig.2a the trend of TC varying the reconstruction is shown and the distance corresponding to the maximum TC is used to reconstruct the BFP (see Fig.2b). Then, coordinates (X_{BFP} ,Y_{BFP}) measure the carrier frequency, thus permitting the hologram demodulation.

2.2 Singular Value Decomposition based filter

The carrier frequency, calculated by implementing the process in the section 2.1, is used to shift the desired diffraction order in the image center. Therefore the input of the proposed SVD-based filter is the shifted amplitude of the Fourier transform of the digital hologram, which will be indicated with **I** in the follow (see Fig.3a). The purpose of the algorithm is to automatically extract the quasi-rectangular shape of the centered diffraction order, preserving the main features of the recorded digital hologram, i.e. without losing informative frequencies with too small filter sizes and at the same time without introducing noisy frequency contributions in case of too large filter sizes.

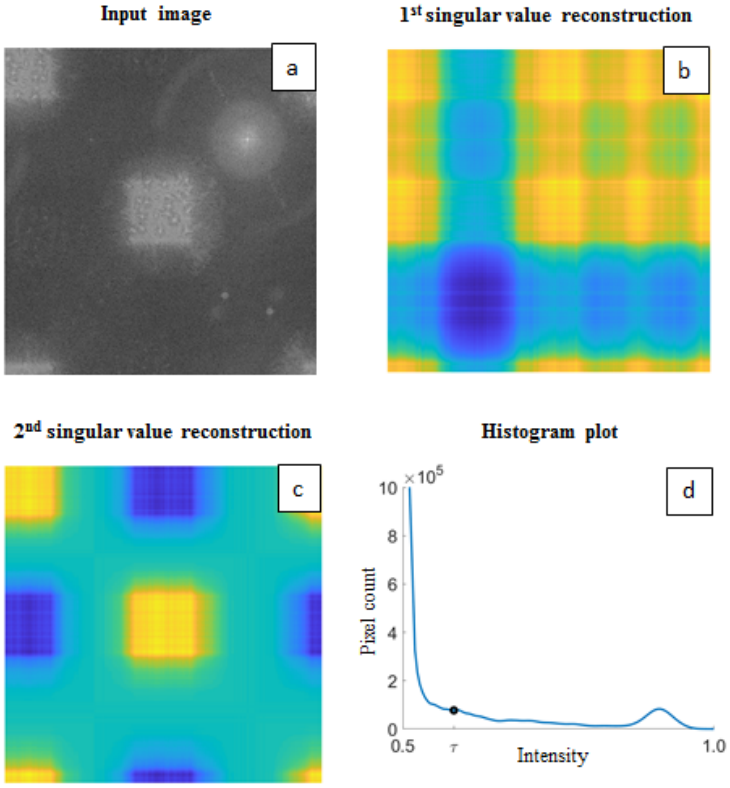

Fig. 3. SVD-based filtering strategy. (a) is the Fourier spectrum in Fig.1b after the demolution using the BFP-based carrier frequency calculation. (b,c) are the 1st and the 2nd singular value reconstructions, obtained by Eq. 2 and (d) is the histogram of the pixel values of (c).

The filtering step consists of the Singular Value Decomposition of **I** [33]:

$$\mathbf{I} = \mathbf{U}\boldsymbol{\Sigma}\mathbf{V}^T = \sum_i \mathbf{u}_i \mathbf{s}_i \mathbf{v}_i^T \tag{2}$$

Where $\mathbf{u}_i$, $\mathbf{s}_i$ and $\mathbf{v}_i$ are the *i*th column of **U**, the *i*th singular value and the *i*th column of **V**. Rank-1approximations of the image can be obtained by separately considering each

contribution of the sum introduced beforehand, as shown in Fig.3, where the first (Fig.3b) and the second (Fig.3c) singular values and vectors are exploited to reconstruct an approximation of **I** [34].
Then, the rank-1 approximation obtained by the second singular value $I_2 = u_2\ s_2\ v_2^T$ is computed and normalized in the range [0,1].
This signal can be effectively used to extract the rectangular-shaped filter for demodulating the hologram with a thresholding operation, so that the filter F can be defined in the following way:

$$F(l,k)=\begin{cases}1 & if\ I_2(l,k)>\tau \\ 0 & otherwise\end{cases} \tag{3}$$

where (l ,k) are the image pixels coordinates and τ is the threshold. Looking at the Fig.3c, the filter should be determined preserving the yellow rectangular shape in the middle of the picture and switching off all the other pixels. The threshold τ is dynamically determined on the histogram of I_2 with an heuristic search, founding a local minimum of the smoothed histogram in the range [0.5, 0.85], thus avoiding the use of a static value. An example of this heuristic search is reported in Fig.3d, in which τ lies in the abovementioned range.
Fig.4a represents the filter F after the thresholding step and the results of a morphological blob analysis performed to filter out noisy portions of the image. This step is needed to detect the best binary mask. The task is performed in two steps: first, let A_{Max} be the area of the largest blob identified on the image, all the blobs with an area value less than $A_{Max}/10$ are filtered out; second, among the remaining blobs, only the one with the centroid closer to the center of the image is considered, while all the other contributions are set to 0. Finally, the output filter F is optionally dilated with a disk of radius ρ, as shown in Fig.4b. Let r be the maximum dimension of the bounding box of the blob, the radius of the disk is set to $\rho=\alpha\cdot r$ (here α=0.05).

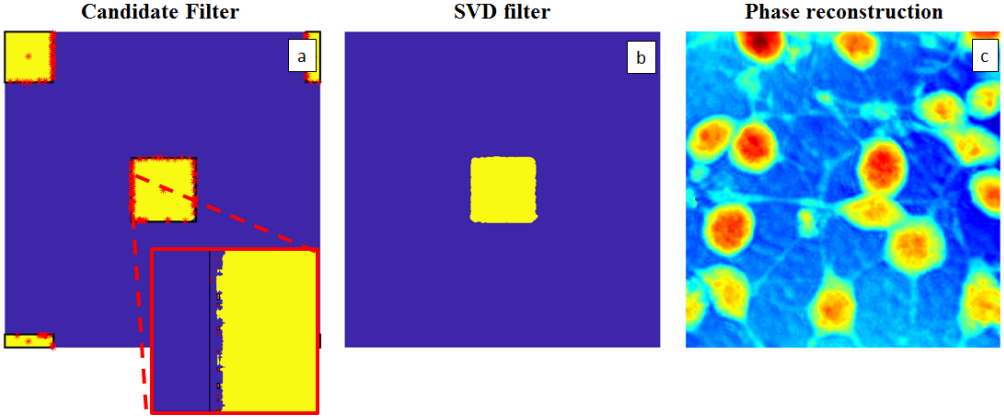

Fig. 4. SVD-based filter correction. (a) is the binary mask obtained after the thresholding procedure in Eq.3. The residual errors highlighted in the zoomed inset are removed a second step of filtering along with an optionally dilated step, obtaining the SVD filter (b). In (c) the phase reconstruction of the digital hologram in Fig.1b, after applying the SVD filter in (b) is reported.

The SVD filter calculated in Fig.4b is used to perform the numerical reconstruction of the digital hologram displayed in the inset of Fig.1b. The resulting phase reconstruction is shown in Fig.4c, demonstrating a remarkable visual quality. Of course, in the next section, we evaluate such quality by quantifying the performance of the proposed SVD based filtering

through a comparison with the classical blind square masking, used on the Fourier spectrum when no information about the reference beam are available.

3. Experimental results

To validate the robustness of the proposed approach, we consider five different digital hologram recording conditions by varying the MO magnification and the resolution and pixels sizes of the CCD sensor. Moreover, we compare the performance of the SVD filtering by a comparison with the classical Blind Fourier Filtering (BFF). Since no a priori information about the reference beam are available, BFF provides a squared binary mask with the side L given by the following rule

$$\frac{L}{2} = \min\left\{X_{BFP}, Y_{BFP}, M - X_{BFP}, N - X_{BFP}, \left|X_{BFP} - X_C\right|, \left|Y_{BFP} - Y_C\right|\right\} \quad (4)$$

where M,N are the image sizes and (X_C, Y_C) are the coordinates of the image center. The comparison is performed on wrapped phase reconstructions obtained by using the BFF and SVD filters, i.e. by evaluating the effect of such filters on the entire reconstruction process. Specifically, after the spectrum filtering, the refocusing criterion based on the TC is applied to calculate the in-focus distance [23], with a scanning step equal to 0.5 μm, then the phase information is extracted from the refocused complex reconstructions. These phase image are affected by aberrations, therefore a 2D quadratic fitting is used to remove them. Different filtering strategies may change the position of the in-focus plane, the aberration compensation process, causing residual aberrations, and the noise level on the wrapped phase reconstructions. Therefore, we consider two metrics ro evaluate the phase images quality, i.e. the Focus Variation (*FV*), calculated as the absolute difference between calculated distances in the two cases, i.e. d_{SVD} - d_{BFF}:

$$FV = \left|d_{SVD} - d_{BFF}\right| \quad (5)$$

and the Noise Level Reduction (*NLR*), evaluated by the following formulas:

$$NLR = \left(1 - \frac{std\left(\Phi_{BFF}\right)}{std\left(\Phi_{SVD}\right)}\right) \cdot 100 \quad (5)$$

where *std*(.) is the standard deviation operator and Φ_{SVD} and Φ_{BFF} are the wrapped phase reconstructions for the two filtering strategies. Finally, the residual aberrations can be simply detected by visual inspection. In Table 1 we summarize the experimental cases analyzed for the comparison, along with FV and NLV. Finally, Fig.5 reports the BFF and SVD filters used in the experiments and the corresponding wrapped phase reconstructions.

Table 1. Experiments' details and performance metrics evaluation

Exp: MO, p_{CCD}, Hologram sizes	*FV* (μm)	*NLR* (%)	Residual Aberrations
Fig.5(a-c): 20x; 7.6μm; 1024x1024	1.0	-40.7	NO
Fig.5(d-f): 20x; 5.5μm; 2048x2048	2.5	---	YES
Fig.5(g-i): 50x; 6.45μm; 1024x1024	0.5	-32.6	NO
Fig.5(j-l): 60x; 5.5μm; 2048x2048	2.0	---	YES
Fig.5(m-o): 100x; 6.7μm; 1024x1024	1.0	---	YES

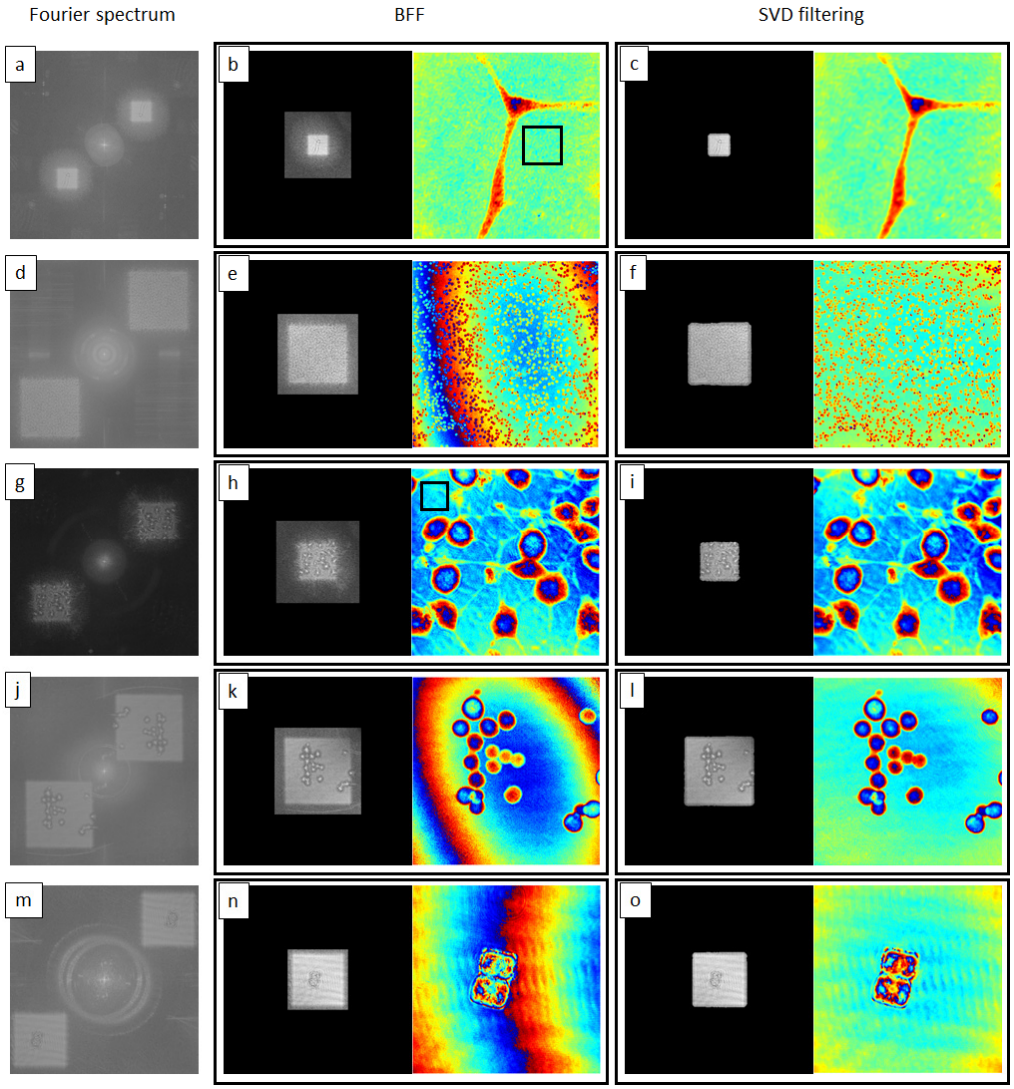

Fig. 5. Comparison between BFF and SVD filtering. (a,d,g,j,m) are the Fourier transform of the corresponding digital hologram. The pairs (b,c), (e,f), (h,i), (k,l) and (n,o) report the BFF and SVD filter applied to shifted spectrums, obtained by using the calculated carrier frequencies, along with the corresponding wrapped phase reconstructions. The black squares within the wrapped phase images in (b,h) highlight the regions used to evaluate the NLR.

In all testes, a small change in the focusing plane is observed (second column of Table 1), while residual aberrations occur for phase reconstructions in Fig.5 e,k,n when the BFF is used. Instead the corresponding images in Fig.5 f,l,o seem to be free form residual aberrations. Finally, the NLR has been evaluated just in cases of the aberrations compensation works efficiently, i.e. for the cases in Fig.5 b,c and Fig.5 h,I, since the NLR can be evaluated only in flat regions. The black squares in Fig.5 b,h highlight regions in which the NLR is calculated, showing a remarkable noise reduction in both cases (see Table 1).
Definitely, in all cases, the SVD filtering is efficient enough to guarantee high quality phase reconstructions, as reported in Fig.5 c,f,i,l,o.

4. Conclusions

We have proposed a new approach, based on the SVD filtering, for the effective and automatic suppression of the zero-order and the twin image in digital holographic reconstruction, in cases of any off-axis configuration recording. Moreover, we have shown that, the proposed approach does not require a priori information about the reference beam's curvature, neither about the off-axis angle (i.e. the spatial carrier frequency). The method has been validated by comparing it with respect to the common BFF in various cases of experimental conditions and for several biological samples. Hence, we demonstrated that, the method is general and robust and it is effective for filtering out to the zero-order and the twin image, also by providing an exact calculation of the carrier frequency of the reference beam through the identification of the BFP of the MO exploiting the sparsity property of digital holograms.

5. Authors contribution

PM and VR contributed equally to this work.

6. References

1. P. Ferraro, A. Wax, and Z. Zalevsky, *Coherent Light Microscopy*, Springer Series in Surface Sciences, **46**, (2011).
2. Y.K. Park, C. Depeursinge, and G. Popescu, "Quantitative phase imaging in biomedicine," Nat. Photonics **12**, 578–589 (2018).
3. M.K. Kim, "Principles and techniques of digital holographic microscopy," SPIE Rev. **1**, 18005 (2010).
4. P. Memmolo, V. Bianco, M. Paturzo, and P. Ferraro, "Numerical Manipulation of Digital Holograms for 3-D Imaging and Display: An Overview," Proc. IEEE, **105**(5), 892-905 (2017).
5. F. Merola, P. Memmolo, L. Miccio, V. Bianco, M. Paturzo, and P. Ferraro, "Diagnostic Tools for Lab-on-Chip Applications Based on Coherent Imaging Microscopy," Proc. IEEE **103**(2), 192 - 204 (2015).
6. Z.S. Ballard, Y. Zhang, and A. Ozcan, "Off-axis holography and micro-optics improve lab-on-a-chip imaging," Light Sci. Appl. **6**, e17105 (2017).
7. V. Bianco, B. Mandracchia, V. Marchesano, V. Pagliarulo, F. Olivieri, S. Coppola, M. Paturzo, and P. Ferraro, "Endowing a plain fluidic chip with micro-optics: a holographic microscope slide," Light Sci. Appl. **6**, e17055 (2017).
8. P. Memmolo, L. Miccio, M. Paturzo, G. Di Caprio, G. Coppola, P.A. Netti, and P. Ferraro, "Recent advances in holographic 3D particle tracking," Adv. Opt. Photon. **7**, 713-755 (2015).
9. X. Yu, J. Hong, C. Liu, and M. K. Kim, "Review of digital holographic microscopy for three-dimensional profiling and tracking," Opt. Eng. **53**, 112306 (2014).
10. F. Merola, P. Memmolo, L. Miccio, M. Mugnano and P. Ferraro, "Phase Contrast Tomography at Lab on Chip scale by Digital Holography," Methods **136**, 108-115 (2018).
11. D. Jin, R. Zhou, Z. Yaqoob and P.T.C. So, "Tomographic phase microscopy: principles and applications in bioimaging [Invited]," J. Opt. Soc. Am. B **34**, B64-B77 (2017).
12. F. Merola, P. Memmolo, L. Miccio, R. Savoia, M. Mugnano, A. Fontana, G. D'Ippolito, A. Sardo, A. Iolascon, A. Gambale and P. Ferraro, "Tomographic Flow Cytometry by Digital Holography," Light Sci. Appl. **6**, e16241 (2017).
13. M.M. Villone, P. Memmolo, F. Merola, M. Mugnano, L. Miccio, P.L. Maffettone and P. Ferraro, "Full-angle tomographic phase microscopy of flowing quasi-spherical cells," Lab Chip **18**, 126-131 (2018).
14. B. Javidi, A. Markman, S. Rawat, T. O'Connor, A. Anand, and B. Andemariam, "Sickle cell disease diagnosis based on spatio-temporal cell dynamics analysis using 3D printed shearing digital holographic microscopy," Opt. Express **26**, 13614-13627 (2018).
15. D.K. Singh, C.C. Ahrens, W. Li, and S.A. Vanapalli, "Label-free, high-throughput holographic screening and enumeration of tumor cells in blood," Lab Chip **17**, 2920-2932 (2017).
16. M. Mugnano, P. Memmolo, L. Miccio, F. Merola, V. Bianco, A. Bramanti, A. Gambale, R. Russo, I. Andolfo, A. Iolascon and P. Ferraro, "Label-Free Optical Marker for Red-Blood-Cell Phenotyping of Inherited Anemias," Anal. Chem. **90**, 7495−7501 (2018).
17. E. Cuche, P. Marquet, and C. Depeursinge, "Spatial filtering for zero-order and twin-image elimination in digital off-axis holography," Appl. Opt. **39**, 4070-4075 (2000).

18. D. Kim, R. Magnusson, M. Jin, J. Lee, and W. Chegal, "Complex object wave direct extraction method in off-axis digital holography," Opt. Express **21**, 3658-3668 (2013).
19. M. Matrecano, P. Memmolo, L. Miccio, A. Persano, F. Quaranta, P. Siciliano, and P. Ferraro, "Improving holographic reconstruction by automatic Butterworth filtering for microelectromechanical systems characterization," Appl. Opt. **54**, 3428-3432 (2015).
20. Z. Dong, H. Wang, and X. Wang "Automatic filtering for zero-order and twin-image elimination in off-axis digital holography," Opt. Eng. **58**(2), 023112 (2019).
21. S. K. Mohammed, L. Bouamama, D. Bahloul, and P. Picart, "Quality assessment of refocus criteria for particle imaging in digital off-axis holography," Appl. Opt. **56**, F158-F166 (2017).
22. Yibo Zhang, Hongda Wang, Yichen Wu, Miu Tamamitsu, and Aydogan Ozcan, "Edge sparsity criterion for robust holographic autofocusing," Opt. Lett. **42**, 3824-3827 (2017).
23. P. Memmolo, M. Paturzo, B. Javidi, P.A. Netti, and P. Ferraro, "Refocusing criterion via sparsity measurements in digital holography," Opt. Lett. **39**, 4719-4722 (2014).
24. T. Colomb, J. Kühn, F. Charrière, C. Depeursinge, P. Marquet, and N. Aspert, "Total aberrations compensation in digital holographic microscopy with a reference conjugated hologram," Opt. Express **14**, 4300-4306 (2006).
25. J. Sun, Q. Chen, Y. Zhang, and C. Zuo, "Optimal principal component analysis-based numerical phase aberration compensation method for digital holography," Opt. Lett. **41**, 1293-1296 (2016).
26. Thanh Nguyen, Vy Bui, Van Lam, Christopher B. Raub, Lin-Ching Chang, and George Nehmetallah, "Automatic phase aberration compensation for digital holographic microscopy based on deep learning background detection," Opt. Express **25**, 15043-15057 (2017).
27. J. M. Bioucas-Dias and G. Valadão, "Phase Unwrapping via Graph Cuts," IEEE Trans. Image Process. **16**(3), 698-709 (2007).
28. J. Bioucas-Dias, V. Katkovnik, J. Astola, and K. Egiazarian, "Absolute phase estimation: adaptive local denoising and global unwrapping," Appl. Opt. **47**, 5358-5369 (2008).
29. W. Xiao, Q. Wang, F. Pan, R. Cao, X. Wu, and L. Sun, "Adaptive frequency filtering based on convolutional neural networks in off-axis digital holographic microscopy," Biomed. Opt. Express **10**, 1613-1626 (2019).
30. T. Pitkäaho, A. Manninen, and T.J. Naughton, "Focus prediction in digital holographic microscopy using deep convolutional neural networks," Appl. Opt. **58**, A202-A208 (2019).
31. T. Nguyen, V. Bui, V. Lam, C.B. Raub, L-C. Chang, and G. Nehmetallah, "Automatic phase aberration compensation for digital holographic microscopy based on deep learning background detection," Opt. Express **25**, 15043-15057 (2017).
32. K. Wang, Y. Li, Q. Kemao, J. Di, and J. Zhao, "One-step robust deep learning phase unwrapping," Opt. Express **27**, 15100-15115 (2019).
33. R.A. Sadek, "SVD Based Image Processing Applications: State of The Art, Contributions and Research Challenges," arXiv:1211.7102 (2012).
34. J.J. Gerbrands, "On the relationships between SVD, KLT and PCA," Pattern Recognit. 14, 375-381 (1981).